Support information

CoF_2 coupled MXene with facile active phase reconstruction for oxygen evolution reaction

Jiayu Xu [a], Qiaowei Wang [a], Shuli Wang [a], Yun Yang [b] *, Ligang Feng [a] *

[a] School of Chemistry and Chemical Engineering, Yangzhou University, Yangzhou 225002, China.

E-mail: ligang.feng@yzu.edu.cn; fenglg11@gmail.com

[b] Nanomaterials and Chemistry Key Laboratory, Wenzhou University, Wenzhou, China. E-mail: bachier@163.com

1. Experimental Section

1.1 Materials

Cobalt nitrate hexahydrate ($Co(NO_3)_2 \cdot 6H_2O$), Ammonium fluoride (NH_4F), Urea (CH_4N_2O), Ti_3AlC_2 (MAX), dicyanodiamide Nafion (5 wt%) were purchased from Sigma-Aldrich. Ethanol was purchased from Sinopharm Chemical Reagent Beijing Co. LTD. All chemicals used were of analytical grade and used without further purification in this study. All solutions were prepared with ultrapure water with a resistance of 18.2 MΩ (Thermo Fisher Scientific Co. LTD, USA).

1.2 Synthesis of the catalysts

1.2.1 Synthesis of $Ti_3C_2T_x$ MXene

$Ti_3C_2T_x$ MXene was fabricated by etching of Ti_3AlC_2 (MAX) powder. In general, Ti_3AlC_2 powder (2 g) was slowly added to 40 % HF solution (30 mL) and stirred for 24 h at room temperature. The resulting product was centrifuged at 3000 rpm for 5 minutes and washed several times with deionized water. Finally, the as-formed product was dried in a vacuum oven at 60 ℃ for 12 h to obtain the $Ti_3C_2T_x$ MXene.

1.2.2 Synthesis of Co(OH)F/MXene

Co(OH)F/MXene was prepared using the oil bath method. First, $Co(NO_3)_2$ $6H_2O$ (1.66 g), NH_4F (0.42 g), and urea (1.71 g) were added to 40 mL of deionized water. It was stirred for 10 min under magnetic stirring conditions, then MXene (0.1 g) was added and sonicated for 45 min to form a homogeneous solution. The mixture was then transferred to a three-necked flask and heated with stirring in an oil bath at 150 ℃ for 6 h. While the suspension was naturally cooled to room temperature, it was washed several times with ultrapure water. The product was collected and dried overnight in a vacuum oven at 60 ℃.

1.2.3 Synthesis of CoF_2/MXene and CoF_2

The obtained Co(OH)F/MXene was subjected to a low-temperature fluorination etching treatment. Co(OH)F/MXene and ammonium fluoride (NH_4F) were placed at two separate positions of a porcelain boat with a mass ratio of 1:10, and NH_4F was placed on the upstream side; then they were heated in a nitrogen atmosphere at 350 °C for 2 h. As a comparison, CoF_2 was prepared by the same method except that no MXene was added during the preparation.

2. Physical characterizations

Powder X-ray diffraction (XRD) patterns were recorded on a Bruker D8 Advance powder X-ray diffractometer using a Cu K_α (λ = 1.5405 Å) radiation source operating at 40 kV and 30 mA at a scanning rate of 5° min^{-1}. The morphology and microstructure of the product were analyzed by scanning electron microscope (SEM, S4800II) and transmission electron microscopy (TEM, Philips, Tecnai 12 F30 S-TWIN). High-resolution TEM (HRTEM) was conducted on a TECNAI G2 operating at 200 kV. X-ray photoelectron spectroscopy (XPS) measurements were carried out on an ESCALAB250Xi spectrometer with an Al K_α radiation source.

3. Electrochemical measurements

All the electrochemical measurements were tested in a typical three-electrode system linked to a Bio-Logic SAS analyzer (France). Our catalysts electrode served as the working electrode with a graphite rod as the counter electrode; a mercury/mercury oxide electrode (Hg/HgO) as the reference electrode was employed through a double salt bridge and lugging capillary and it was calibrated before and after the experiments to ensure the accuracy. A glassy carbon electrode (GCE, 3.0 mm diameter) was used to support the catalysts. The working electrode was prepared as follows: 5 mg of catalysts was dispersed entirely into the mixture of 50 μL Nafion and 950 μL ethanol and ultrasonicated for 30 min to form a uniform catalyst suspension. Then, 10 μL of the catalyst suspension was loaded dropwise to the GCE. The prepared working electrode was placed in 1 M KOH and treated with N_2 for electrochemical testing. All the potentials used were converted into RHE: ($E_{(RHE)} = E_{(Hg/HgO)}$ +0.0591*pH+0.098 V). The catalytic performance of the samples for OER was evaluated by linear scan voltammetry (LSV), and the scanning rate was 5 mV s^{-1}.

The electrochemical impedance spectroscopy (EIS) frequency range was 1000 kHz ~ 0.01Hz. The chronoamperometry (CA) was measured at a constant potential of 1.51 V vs RHE for 10 h. All tests were carried out at room temperature (around 25 °C) and all LSV curves were corrected without iR compensation.

To estimate the effective surface areas of catalysts, we measured the double-layer capacitance (C_{dl}) by cyclic voltammetry (CV) method by varying the scan rate (20, 40, 60, 80, and 100 mV s^{-1}) in the non-Faradaic region from 0.89 to 0.99 V vs RHE. By plotting $\Delta j = 1/2\ (j_{anodic} - j_{cathodic})$ at the middle potential (0.94 V) against the scanning rates, the linear slope is C_{dl}. j_{anodic} and $j_{cathodic}$ are anodic and cathodic current densities at the anode (>0) and cathode (<0), respectively. The electrochemical active surface

area (ECSA) was achieved by normalizing the C_{dl} to a standard-specific capacitance. ECSA was calculated according to the following equations S1, 40 μF cm^{-2} was adopted as the specific capacitance (C_s) value as regards previous reports [1, 2], and S is the surface area of the electrode (0.07 cm^{-2}):

$$ECSA = \frac{C_{dl} * S}{C_s}$$

Equation S1:

The turnover frequency (TOF) values were calculated from the equation S2:

$$TOF = \frac{j * S}{4 * F * m}$$

Equation S2:

Where j is the current density at a specific potential, F is the Faraday constant (96485 C mol^{-1}) and m is the number of moles of active materials.

4. Density functional theory (DFT) calculation

DFT calculations were performed using the CASTEP module of the Materials Studio software (Accelrys Inc.). The generalized gradient approximation method (GGA) with the Perdew-Burke-Ernzerhof (PBE) functional was used to describe the exchange and correlation interactions [3, 4]. The interactions between valence electrons and ionic cores were described by Ultrasoft pseudo-potential and dispersion adjustment using DFT-D correction. The electronic wave functions were expanded on a plane wave basis with a cut-off energy of 380 eV, and the self-consistent field (SCF) tolerance is 1.0×10^{-6} eV/atom. The optimization is completed when the energy, maximum force, maximum stress, and maximum displacement are less than 5.0×10^{-6} eV/atom, 0.01 eV/Å, 0.02 GPa, and 5.0×10^{-4} Å, respectively. A vacuum slab with a thickness greater than 15 Å was used in the z-direction. The Gibbs free energy of the reaction and Gibbs free energy of the adsorption intermediate can be obtained from equation S3 [5]:

Equation S3: $\Delta G = \Delta E + \Delta ZPE - T\Delta S$

where ΔE is the energy of the reaction, ZPE is the zero-point energy change, and ΔS is the entropy change.

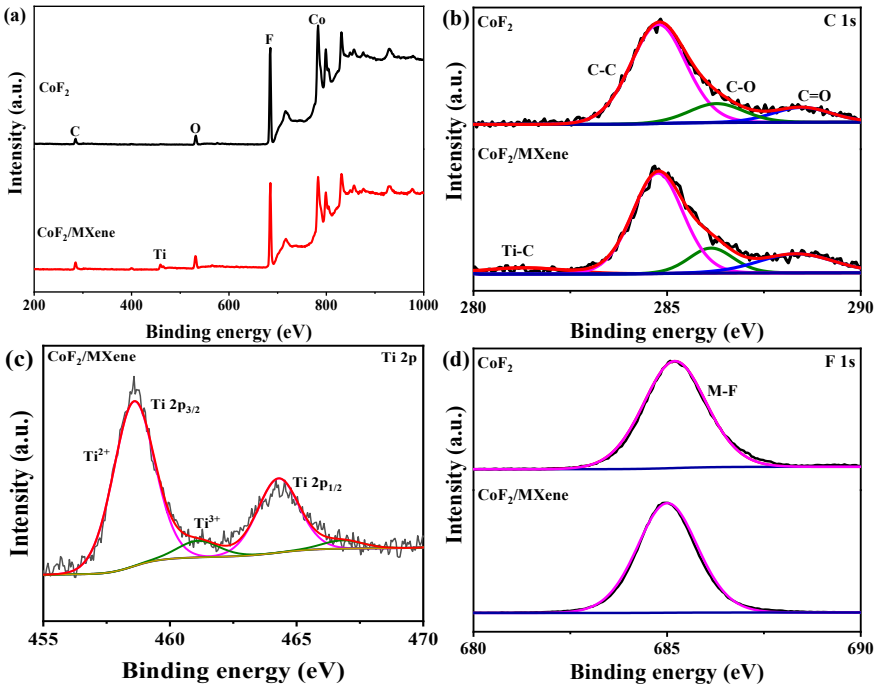

Fig. S1. (a) The XPS survey spectra; High-resolution XPS spectrum for (b) C 1s; (c) Ti 2p and (d) F 1s of CoF_2 and CoF_2/MXene.

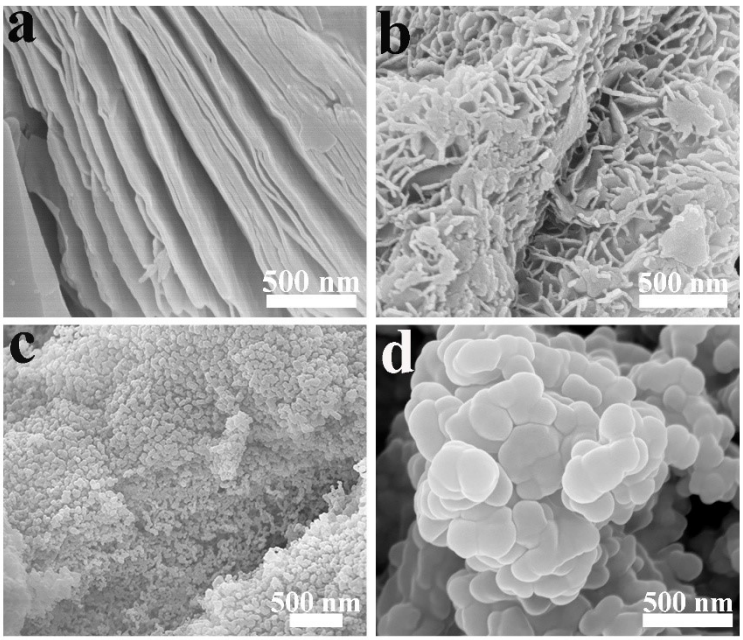

Fig. S2. The SEM images of (a) MXene, (b) Co(OH)F/MXene, (c) CoF_2/MXene and (d) CoF_2 samples.

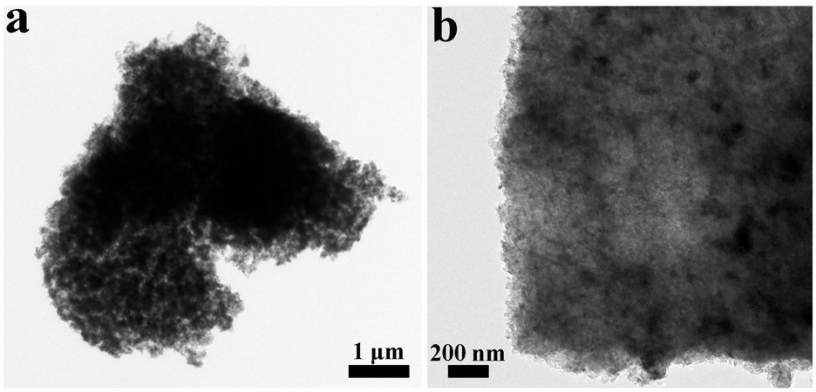

Fig. S3. The TEM images of (a-b) CoF_2/MXene sample.

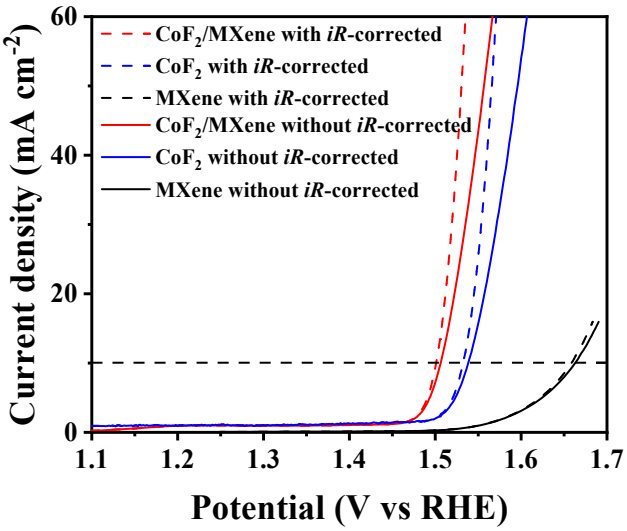

Fig. S4. Polarization curves for OER with and without *iR* correction.

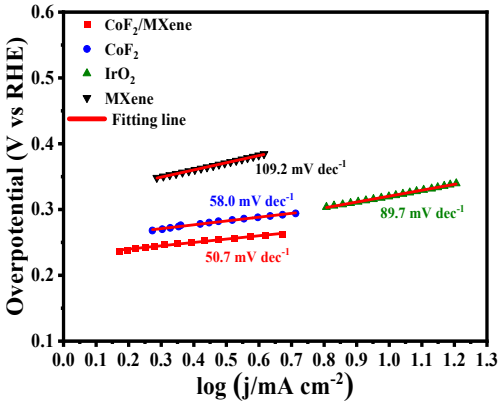

Fig. S5. The Tafel splot of CoF_2/MXene, CoF_2, MXene and IrO_2.

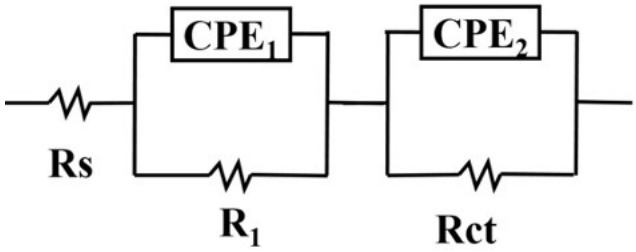

Fig. S6. Equivalent circuit diagram for fitting the EIS data.

R_s means uncompensated solution resistance, R_{ct} is a charge transfer resistance, R_1 is associated with the contact resistance between the catalysts, and the CPE generally was employed to well fit the impedance data by safely treating it as an empirical constant without considering its physical basis. And mostly, it was regarded as the double-layer capacitor from the catalyst/support and catalyst solution.

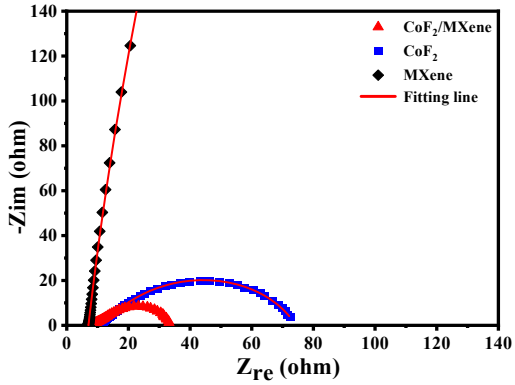

Fig. S7. Nyquist plots of the CoF_2/MXene, CoF_2 and MXene.

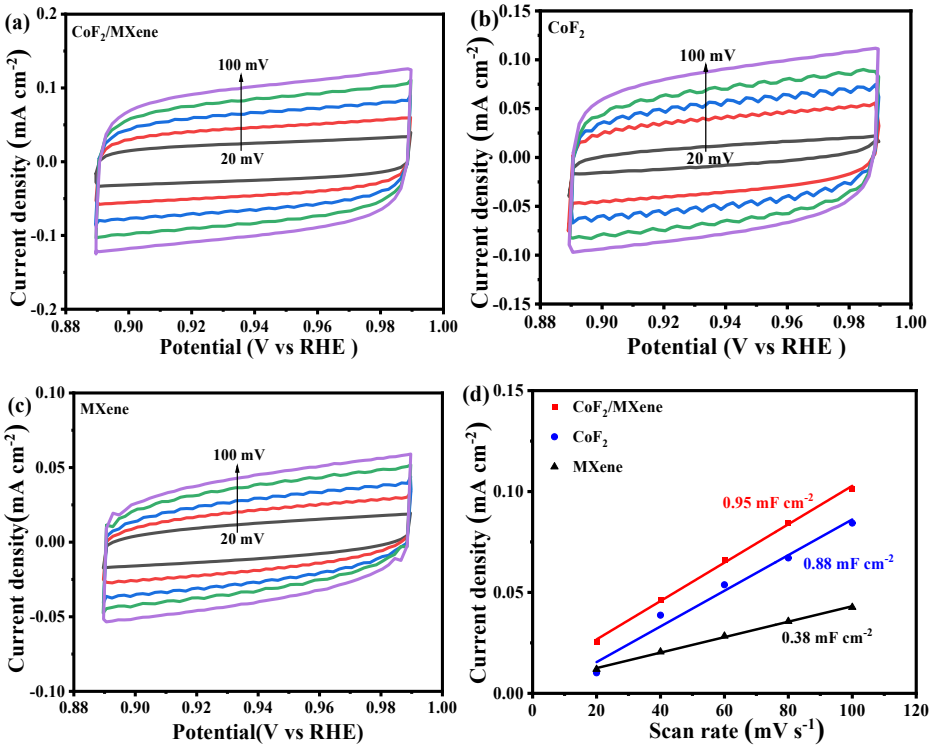

Fig. S8. CV curves of (a) CoF_2/MXene, (b) CoF_2 and (c) MXene samples in the non-faradaic capacitance current range from 0.89 V to 0.99 V (vs RHE) at scan rates of 20, 40, 60, 80 and 100 mV s^{-1}. (d) The C_{dl} values of CoF_2/MXene, CoF_2 and MXene samples.

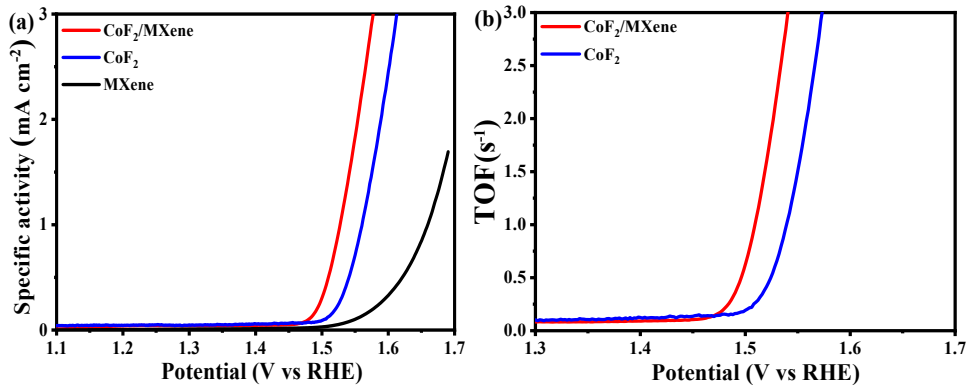

Fig. S9. (a) The specific activity of CoF_2/MXene, CoF_2 and MXene samples. (b) TOF curves of CoF_2/MXene and CoF_2.

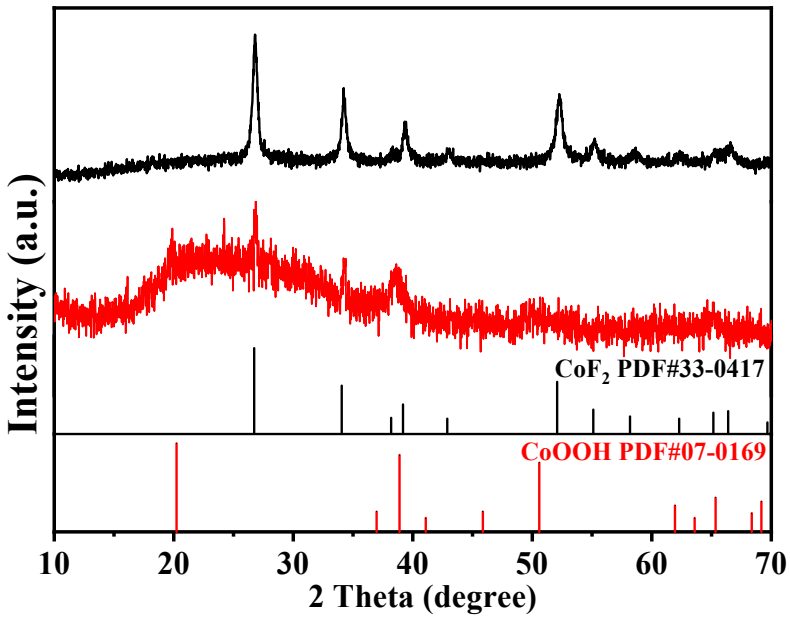

Fig. S10. The XRD pattern of CoF_2/MXene before and after the OER test.

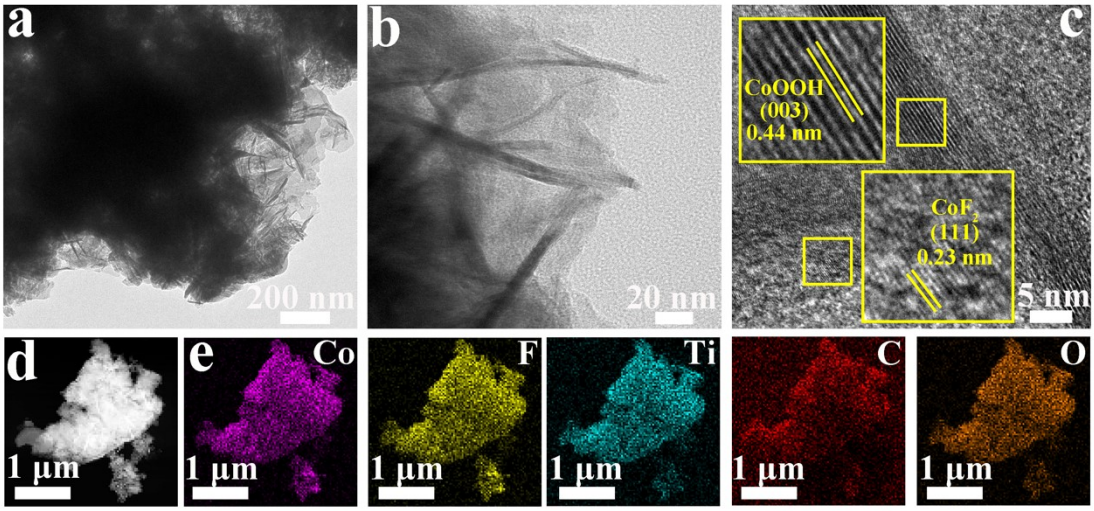

Fig. S11. (a-b) TEM images, (c) HRTEM image, (d) STEM image and (e) elemental mappings of CoF_2/MXene after the OER test.

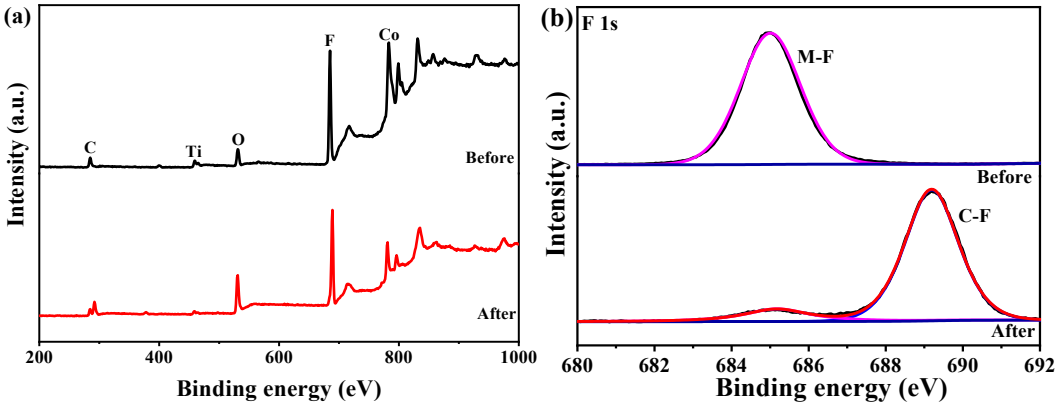

Fig. S12. (a) The XPS survey spectra; (b) High-resolution XPS spectrum for F 1s before and after the OER test for CoF_2/MXene.

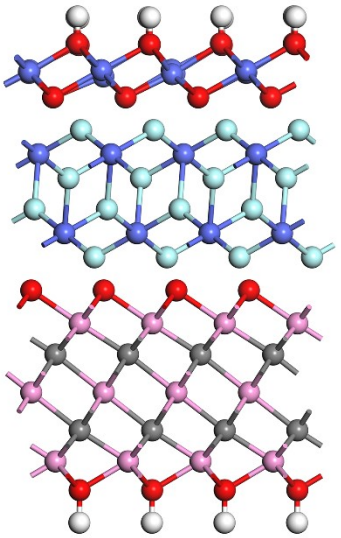

Fig. S13. The optimized models with a layer of CoOOH covered on the surface of CoF_2/MXene.

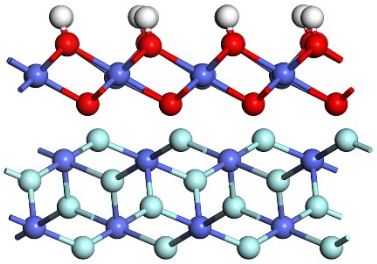

Fig. S14. The optimized models with a layer of CoOOH covered on the surface of CoF_2.

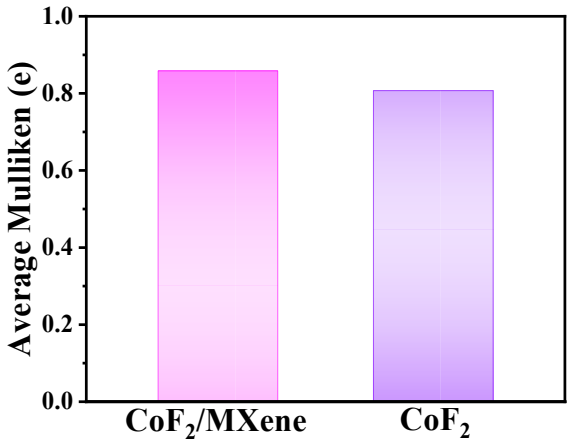

Fig. S15. The average Mulliken charge of Co of the CoF_2/MXene and CoF_2.

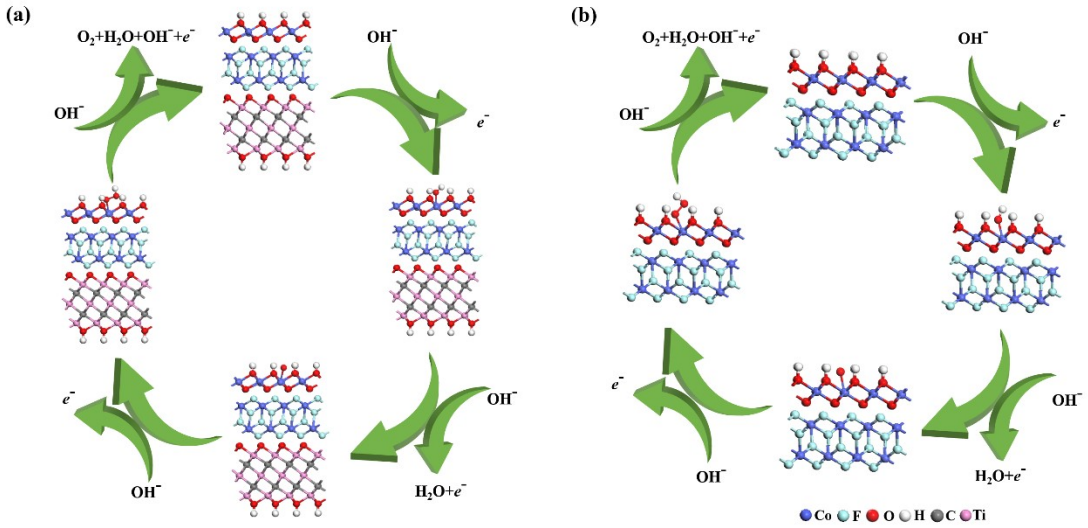

Fig. S16. A model for the adsorption of reaction intermediates on (a) CoF_2/MXene and (b) CoF_2 surfaces.

Table S1 The detailed binding energy of Co elements of the CoF_2/MXene and CoF_2 sample.

Catalysts	Co $2p_{3/2}$		Co $2p_{1/2}$		Relative content/%
	Peak	Binding energy/eV	Peak	Binding energy/eV	
CoF_2/MXene	Co-O	781.7	Co-O	797.9	19.7%
	Co-F	783.2	Co-F	799.4	80.3%
CoF_2	Co-O	781.5	Co-O	797.7	11.0%
	Co-F	783.0	Co-F	799.2	89.0%

Table S2. The comparison of other OER catalysts derived from the Co-based catalysts in 1 M KOH.

Catalysts	Electrode substrate	Overpotential η_{10} (mV)	Tafel splots (mV dec^{-1})	Reference
CoF_2/MXene	GCE	275	50.7	This work
CoNi MOF-mCNTs	GCE	306	42	[6]
AC-FeCoNi	GCE	279	58	[7]
O-Co/NiCoP	carbon cloth	330	66	[8]
NiCoFe-HO@NiCo-LDH YSMRs	GCE	278	49.7	[9]
FeCoNi-NC	GCE	310	20	[10]
Co/NMHCS (900)	GCE	274	51.4	[11]
FeNiCo	GCE	260	42	[12]
Co/Fe-SNC800	carbon cloth	240	47.9	[13]
CoNiFe LTHs	GCE	262	88.1	[14]
Co/CoFeNC@N-CNF	GCE	320	81	[15]
$Co(OH)_2/V_2O_5$	GCE	320	68	[16]
CoFeP@C	GCE	336	82.5	[17]
Fe-CoNi LDHs	GCE	260	49	[18]
Ar-CoFe PBA	GCE	305	36.1	[19]
$Fe_{1.0}Co_{1.1}Ni_{1.4}$–NC	GCE	270	60	[20]

Table S3. EIS fitting parameters from equivalent circuits for CoF_2/MXene, CoF_2 and MXene samples in 1 M KOH.

Samples	R_s/Ω	R_{ct}/Ω	R_1/Ω	Chi squared
CoF_2/MXene	8.8	20.3	32.1	1.236E-03
CoF_2	10.1	63.2	18.1	7.615E-05
MXene	7.3	3680	3257	6.875e-04

Table S4. C_{dl} and ECSA for CoF_2/MXene, CoF_2 and MXene samples in 1 M KOH.

Catalysts	**C_{dl} (mF cm^{-2})**	**ECSA (cm^2)**
CoF_2/MXene	0.95	1.66
CoF_2	0.88	1.54
MXene	0.38	0.66

Table S5. Mulliken charge (e) of each Co and F atoms in CoF_2/MXene and CoF_2.

Atom	CoF_2/MXene	CoF_2
Co	0.92	0.92
Co	0.86	0.87
Co	0.92	0.86
Co	0.83	0.83
Co	0.92	0.89
Co	0.84	0.86
Co	0.91	0.89
Co	0.83	0.82
Co	0.89	0.91
Co	0.88	0.84
Co	0.92	0.89
Co	0.89	0.80
Co	0.92	0.92
Co	0.87	0.83
Co	0.91	0.89
Co	0.89	0.82
Co	0.91	0.80
Co	0.90	0.79
Co	0.69	0.73
Co	0.88	0.80
Co	0.83	0.80
Co	0.65	0.80
Co	0.63	0.59
Co	0.83	0.80
Co	0.85	0.79
Co	0.91	0.79
Co	0.85	0.73
Co	0.90	0.80
Co	/	0.60
Co	/	0.65
Co	/	0.73
Co	/	0.79
F	-0.32	-0.55
F	-0.48	-0.48
F	-0.48	-0.50
F	-0.33	-0.11
F	-0.41	-0.48
F	-0.47	-0.46
F	-0.47	-0.49
F	-0.13	-0.29
F	-0.31	-0.55
F	-0.48	-0.48

F	-0.48	-0.50
F	-0.33	-0.12
F	-0.41	-0.48
F	-0.47	-0.46
F	-0.47	-0.49
F	-0.14	-0.29
F	-0.42	-0.55
F	-0.47	-0.48
F	-0.47	-0.50
F	-0.20	-0.12
F	-0.34	-0.48
F	-0.47	-0.46
F	-0.47	-0.49
F	-0.40	-0.29
F	-0.42	-0.55
F	-0.47	-0.48
F	-0.47	-0.50
F	-0.20	-0.12
F	-0.33	-0.48
F	-0.47	-0.46
F	-0.47	-0.49
F	-0.40	-0.30

References:

1. X. Gu, Z. Liu, M. Li, J. Tian and L. Feng, *Appl. Catal., B*, 2021, **297**, 120462.
2. X. Gu, Z. Liu, H. Liu, C. Pei and L. Feng, *Chem. Eng. J.*, 2021, **403**, 126371.
3. Y. Feng, S. Lu, L. Fu, F. Yang and L. Feng, *Chem. Sci.*, 2024, **15**, 2123-2132.
4. D. Vanderbilt, *Physical Review B*, 1990, **41**, 7892-7895.
5. J. Xu, L. Yu, B. Dong, F. Yang and L. Feng, *J. Colloid Interface Sci.*, 2023, **654**.
6. S. Yu, Y. Wu, Q. Xue, J.-J. Zhu and Y. Zhou, *J. Mater. Chem. A*, 2022, **10**, 4936-4943.
7. Y. Hu, G. Luo, L. Wang, X. Liu, Y. Qu, Y. Zhou, F. Zhou, Z. Li, Y. Li, T. Yao, C. Xiong, B. Yang, Z. Yu and Y. Wu, *Adv. Energy Mater.*, 2021, **11**, 2002816.
8. Y. Lin, X. Cui, Y. Zhao, Z. Liu, G. Zhang and Y. Pan, *Nano Res.*, 2023, **16**, 8765-8772.
9. Q. Niu, M. Yang, D. Luan, N. W. Li, L. Yu and X. W. Lou, *Angew. Chem. Int. Ed.*, 2022, **61**, e202213049.
10. X. Tang, R. Cao, L. Li, B. Huang, W. Zhai, K. Yuan and Y. Chen, *J. Mater. Chem. A*, 2020, **8**, 25919-25930.
11. J. Diao, S. Wang, Z. Yang, Y. Qiu, R. Xu, W. Wang, K. Chen, X. Li, T. Chao, X. Guo and Y. Qu, *Adv. Mater. Interfaces*, 2023, **10**, 2202394.
12. M. Nishimoto, S. Kitano, D. Kowalski, Y. Aoki and H. Habazaki, *ACS Sustain. Chem. Eng.*, 2021, **9**, 9465-9473.
13. C. Chen, M. Sun, F. Zhang, H. Li, M. Sun, P. Fang, T. Song, W. Chen, J. Dong, B. Rosen, P. Chen, B. Huang and Y. Li, *Energy Environ. Sci.*, 2023, **16**, 1685-1696.

14. R. Yu, D. Liu, M. Yuan, Y. Wang, C. Ye, J. Li and Y. Du, *J. Colloid Interface Sci.*, 2021, **602**, 612-618.
15. J. Li, T. Tan, Y. Xie, J. Chu, L. Li, B. Ouyang, E. Kan and W. Zhang, *J. Colloid Interface Sci.*, 2023, **640**, 78-90.
16. J. Tang, Q. Ruan, H. Yu and C. Huang, *Advanced Sustainable Systems*, 2023, **7**, 2200473.
17. L. Gao, S. Chang and Z. Zhang, *ACS Appl. Mater. Interfaces*, 2021, **13**, 22282-22291.
18. Y. Shi, J. Li, B. Zhang, S. Lv, T. Wang and X. Liu, *Appl. Surf. Sci.*, 2021, **565**, 150506.
19. F. Diao, M. Rykær Kraglund, H. Cao, X. Yan, P. Liu, C. Engelbrekt and X. Xiao, *J. Energy Chem.*, 2023, **78**, 476-486.
20. M. Khalid, A. M. B. Honorato, G. Tremiliosi Filho and H. Varela, *J. Mater. Chem. A*, 2020, **8**, 9021-9031.